Journal of Power Sources 273 (2015) 312–316

Contents lists available at ScienceDirect

Journal of Power Sources

journal homepage: www.elsevier.com/locate/jpowsour

Short communication

Morphologically controlled fuel cell transport layers enabled via electrospun carbon nonwovens

Devin Todd, Walter Mérida*

Clean Energy Research Centre, The University of British Columbia, 2054-6250 Applied Science Lane, Vancouver, BC V6T 1Z4, Canada

HIGHLIGHTS

- We present novel PEM fuel cell transport layers produced via electrospinning.
- Electrospinning enables transport layers produced with varying morphology.
- Electrospun and commercial transport layers are compared ex-situ and in-situ.
- Electrospun transport layers achieve currents 85% that of commercial materials.
- Electrospun transport layers demonstrate more stable output at higher currents.

ARTICLE INFO

Article history:
Received 11 August 2014
Received in revised form
12 September 2014
Accepted 13 September 2014
Available online 22 September 2014

Keywords:
Electrospinning
Fuel cell
Transport layer
Characterization
Proton exchange membrane
Carbon nonwoven

ABSTRACT

We report on the synthesis and performance of carbon nanofibre substrates for PEM fuel cell transport layer applications. Electrospinning is used for fabrication; by manipulation of spinning properties, morphological control is demonstrated in the product. Our application of the technology and it's manipulability to PEMFC transport layers constitutes a novel approach to the manufacture of such layers. Ex-situ morphology, electrical resistance and water contact angles are reported in additional to in-situ hydrogen/air fuel cell performance. Electrospun transport layers are compared directly to established commercial products in a cathode PTL role. The electrospun transport layers demonstrate approximately 85% of the commercial limiting current density, swifter water transport characteristics, and markedly more stable operating points.

1. Introduction

Proton-exchange membrane fuel cells (PEMFCs) are viable energy conversion devices for a growing number of applications – from transportation electrification to portable devices, to stationary energy storage and recovery. The porous transport layers (PTLs), interposed between catalyst layers and bi-polar plates, are a critical component of the PEMFC.

Our group is studying the novel application of electrospinning technology for the synthesis of PEMFC transport layers (both PTL substrates and/or micro-porous layers); with the specific objective of leveraging the technology's unique capacities to engineer the morphology of the layers.

The purpose of the PTLs is to enable electronic, thermal and mass transport between PEMFC sub-components. Carbon fibre based papers, felts and textiles are commonly utilized materials; these may be impregnated with hydrophobic agents and/or have micro-porous layers (MPLs) applied. In contrast to catalyst layers, the development of new PTL structures has received little attention, and the research of transport layers appears focused on the characterization of established materials. Our research is focused on alleviating the deficiencies and improving the performance of conventional PTL materials, while providing greater system optimization opportunity.

Electrospinning is a scalable technique for the preparation of fibres via acceleration of a precursor solution (dope) through an electrical field. The technique has been applied in: filtration, textiles, electronics, energy devices and bio-medicine. The greatest advantages of electrospinning are its minimalism and versatility: fibres or fibre non-woven layers may be produced

* Corresponding author. Tel.: +1 604 822 4189; fax: +1 604 822 2403.
E-mail address: walter.merida@ubc.ca (W. Mérida).

http://dx.doi.org/10.1016/j.jpowsour.2014.09.095
0378-7753/

with variable morphology, be derived from nearly any polymer solution or melt, or be functionalized by inclusion of additives in the dope. Extensive reviews are available in the literature [1,2]. The minimalism of electrospinning is characterized by the simplicity of the basic apparatus: a dope pumping device with capillary tip, a grounded target, and a high-voltage power supply biasing the two.

Applied towards PEMFCs, electrospinning has been the basis of materials for novel catalyst layers [3–7], and membranes [8–10]. Further review is offered by Cavaliere et al. [11] and Dong, Kennedy and Wu [12] whom address energy applications of electrospinning in general.

Unlike the current state-of-the-art, the electrospun transport layers can be designed with properties (e.g.: porosity, hydrophobicity, or conductivities) which vary continuously or in a prescribed manner in three-dimensions; contemporary literature attempting such manipulation in PEMFC PTLs, none of which incorporate electrospinning, have featured composite or gradient MPLs [13–16] and collages of commercial PTLs [17]. Moreover, electrospun layers may incorporate MPL and PTL functionality in a monolithic, hierarchical, structure whilst avoiding discontinuities and irreproducible interactions at interfaces (e.g.: due to rolling, transfer, or pressing manufacturing processes). Electrospinning might also facilitate periodic or global property variation to match bipolar plate topologies, facilitating energy and mass transport between lands-channels or mediating active area operational gradients. The challenge facing electrospun transport layers is the complexity of the electrospinning process. Though the process can be described in simple terms, predicting and/or controlling the electrospun layer structure and composition can be challenging because the final product is sensitive to numerous parameters.

Our survey of the literature reveals two examples of electrospun transport layers applied to PEMFCs. The first is from Duan et al. [18], who manufactured an MPL on a commercial substrate and compared its performance against a self-made conventional MPL. The second is from Hung et al. [19], who implemented an externally sourced electrospun mat in a study comprising several differently manufactured PTLs; no information was offered upon the electrospinning process parameters. Critically, these two studies did not report morphological permutations of the electrospun layer, nor was there recognition of PTL optimization avenues presented by the technology.

We report on the morphology, electronic resistance, interfacial water contact angle, and in-situ PEMFC performance of nonwoven carbon fibre transport layers produced by electrospinning. These layers are produced with different average fibre diameters via manipulation of electrospinning dope composition. We believe our effort is the first published instance where electrospun materials with controlled morphology are applied in a PEMFC transport layer role.

The PTL contribution to PEMFC resistance overpotential is often overlooked as the membrane is the dominant impediment to charge transport in a PEMFC. However, this dominance decreases as optimum humidity conditions are achieved and the resistance contribution of the PTL may remain correlatable to cell performance [20]. For our experimental materials, heat-treatment temperatures are low compared to those used for conventional PTLs [20,21]. This may yield less graphitization and higher resistivities, thus the need to evaluate this property.

Ex-situ resistance notwithstanding, electrospun transport layers may confer worthwhile in-situ performance, particularly in the mass-transport domain. We report the in-situ performance from a hydrogen/air PEM research cell. Results are directly compared to membrane electrode assemblies (MEAs) comprising commercial PTLs.

2. Method

2.1. Materials

Polyacrylonitrile (PAN) (approx. 1,50,000 Mw) was obtained from Scientific Polymer Products and dimethylformamide (DMF) (≥99.9%) from Fisher Scientific. These materials were used without further preparation.

2.2. Sample preparation

PAN was dissolved into DMF to produce solutions of specific polymer percent weights. The solutions were stirred at elevated temperature to ensure a homogeneous mixture, and then allowed to cool to room temperature. Electrospinning was performed using an apparatus from Kato tech Co. (Kyoto, Japan). The system was configured with a voltage bias of 12 kV, a 16 cm tip-to-target distance, 18 g capillary tip, and a foil covered drum target moving at 1 cm s^{-1} surface speed. The capillary tip was traversed over 14.0 cm at 2.00 cm min^{-1}. Dope delivery rate averaged 0.033 mL min^{-1}. Raw spun material was detached from their foil and sandwiched between alumina plates for heat-treatment in a tube furnace. Stabilization was achieved at 240 °C with a 1 °C min^{-1} ramp rate, sustained for 2 h under an air atmosphere. Carbonization was achieved at 900 °C with a 5 °C min^{-1} ramp rate, sustained for 1 h under an argon atmosphere.

2.3. SEM and contact angle analysis

Fibre diameters of the electrospun material were determined both before and after heat-treatment. Images were acquired from a Hitachi S3000N scanning electron microscope, and dimensions analyzed using ImageJ software. Example micrographs are offered in Fig. 1. Water contact angles were acquired via sessile drop experiment. These angles may be used to quantify the PTL hydrophilicity or hydrophobicity, but their applicability is limited to the interaction of macroscopic water droplets with the PTL surface.

2.4. Electrical resistance and mechanical characterization

Through-plane resistance was acquired from apparatus developed in-house. The functional components of the system include: four-point probe arrangement affixed to gold-plated anvils, load cell and pneumatic cylinder. An Agilent 34420A micro-ohm meter delivers resistance measurement. Fig. 2 is a schematic of the system. Electronic area resistance was obtained with a singular sample between anvils and includes the contact contributions of two sample–anvil interfaces. Samples are compressed step-wise in load with pauses to equilibrate at each step.

2.5. In-situ characterization

A 2.25 cm^2 active area hydrogen/air PEMFC coupled to a Greenlight Innovation G20 test station was used to collect in-situ performance data. MEAs incorporated Gore PRIMEA catalyst coated membranes and SGL 25 BC anode PTLs; the cathode PTLs were either our electrospun layers or SGL 25 AA. The cell was operated in potentiostatic mode at 70 °C and 100% relative humidity, with hydrogen/air flow-rates of 0.060/0.200 NLPM.

3. Results and discussion

Fibre diameters in the free-standing nonwovens before and after heat-treatment are reported in Fig. 3. As polymer concentration increases, an increase in fibre diameters is observed. This is

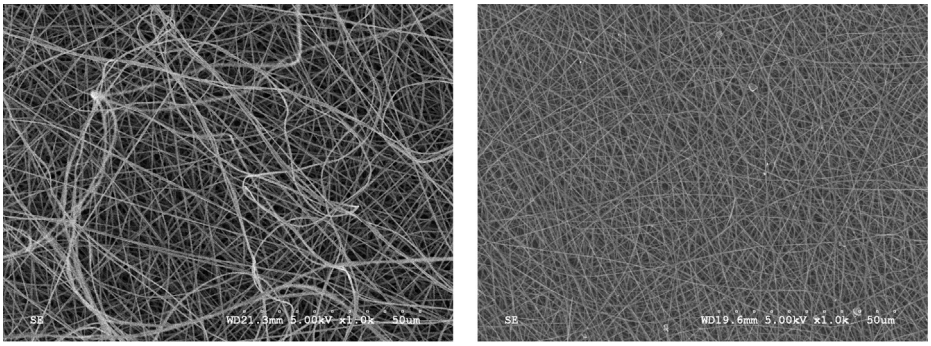

Fig. 1. Typical SEM micrographs of electrospun layers (a) pre-heat-treatment and (b) post-heat-treatment.

consistent with the literature and may be attributed to increased polymer chain entanglement at higher concentrations, producing greater solution viscosities, which in-turn impact the spinning process [2]. The stabilization and carbonization of the raw fibres produced an average diameter reduction of 190 nm. Following Fig. 3, a subset of layers with PAN dope concentrations of 10 and 12.5% were selected for further study; these layers were remanufactured with an approximate 38 μm finished thickness. This selection of concentrations would yield appreciably different fibre diameters whilst the moderate dope viscosities facilitate electrospinning. Due to relative humidity variations, fibre diameters of the thicker layers do not lie upon the original curve but follow a similar trend with polymer concentration. Upon examining the morphology, we observe our synthesis yields a continuous fibre nonwoven without defects at the fibre (i.e. broken fibres and shives) or layer (i.e. cracks) levels. We hypothesize that the continuous fibre morphology may reduce the occurrence of cell damage compared to MEAs with carbon paper transport layers without MPLs, where individual fibres may punch holes through membranes.

Electrical area resistance of the PTLs is plotted in Fig. 4. As spinning dope polymer concentration increases, there appears to be a trend towards lower resistances. We avoid speculation on whether the effect manifests in the bulk material or the contact interfaces, as a rigorous distinction between contact resistance and material resistivity is unavailable. The resistances of our materials are acceptable for transport layer application when compared to membrane contributions which remain dominant at approximately 2×10^{-5} Ω m^2 (Nafion 117, DuPont); suggesting that the peak temperature used for carbonization is effective. Indeed, permutations to our manufacturing process, such as incorporation of conductive additives (e.g.: carbon nano-tubes) to the spinning dope, may improve conductivity. However specific strategies must contend with the parameter sensitivity of the electrospinning process [22] (e.g.: increasing the current carrying of the dope and consequently altering product morphology). Notably, the electrospun PTLs were not visibly damaged during compression. A concern was breakage (e.g.: crumbling) of the layers, whose susceptibility is a function of carbonization temperature. This concern was ultimately placated when electrospun layers were found unbroken post in-situ testing.

Polarization curves from MEAs incorporating the electrospun PTLs are produced in Fig. 5. Addressing each of the kinetic, ohmic and mass-transport domains in-turn: We observe no difference in the kinetic domain for the different transport layer configurations; as should be the case without catalyst layer manipulation. The ohmic domain suggests greater resistance in MEAs using electrospun transport layers versus the commercial baseline. Of the electrospun transport layers, we observe no appreciable difference between the 10 and 12.5% PAN. This is congruent with the results from ex-situ area resistance characterization. The relative difference in ohmic contributions in-situ between commercial and electrospun implementations is not as great as that from ex-situ characterization; but a more appreciable difference between the two electrospun layers might have been anticipated in-situ. Certainly the large ionic resistance of the membrane is a buffer;

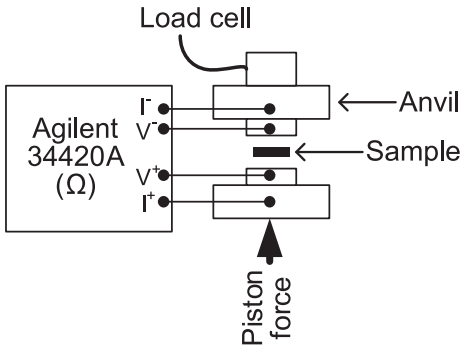

Fig. 2. Schematic of apparatus for electrical area resistance measurement. Components include: anvils for sample engagement, pneumatic cylinder for closing sample, load sensor and Agilent 34420A meter. Excluding the meter, these are located within the bore of a tubular body (not shown for clarity).

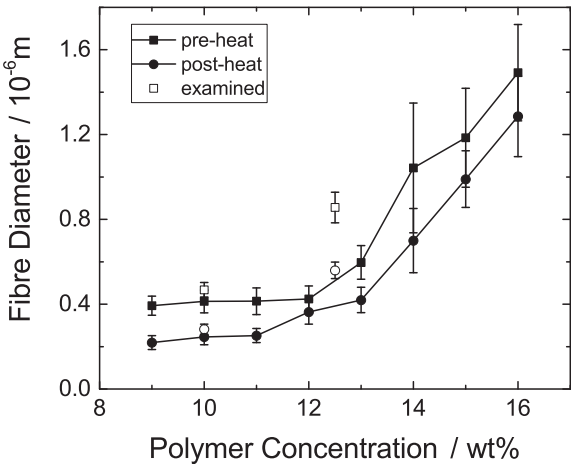

Fig. 3. Plot of fibre diameter as a function of polymer concentration in the electrospinning dope.

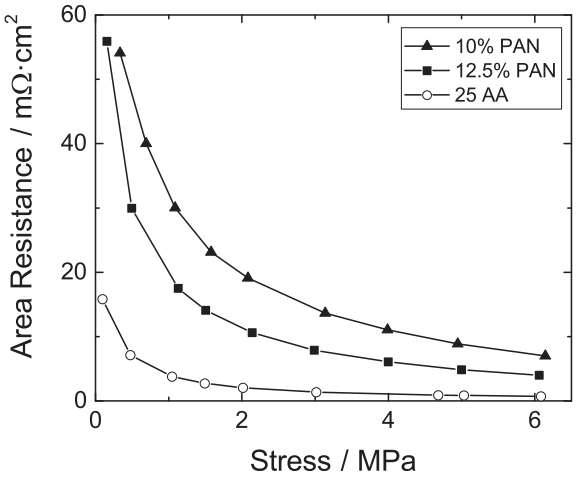

Fig. 4. Area resistance as a function of applied stress for experimental materials (post-heat-treatment) and commercial PTL.

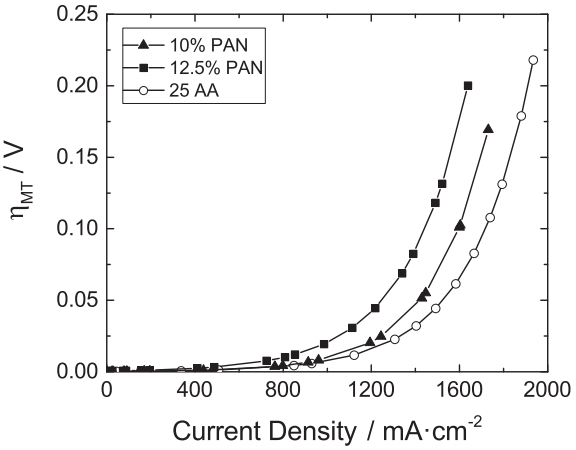

Fig. 6. Mass-transport overpotentials of the different MEAs calculated from a voltage breakdown analysis.

but other effects manifest in-situ which may confound the cell resistance contributions: the membrane resistance is a function of hydration and is inextricably linked to water-transport (and the transport media); the inter-component contact resistances which are structure sensitive; and the distribution of compressive stress, a function of cell and material design. In our experiments the MEAs with electrospun cathode transport layers are thinner than the commercial baseline. It is thought these interact with the cell design (which is optimized for commercial MEAs) to lower overall electrical connectivity between components. The lower connectivity and the proportionally small contribution of PTLs to the total resistance would produce the in-situ similarity between electrospun PTLs, but dissimilarity to the commercial product.

The electrospun transport layers produce approximately 85% of the limiting current density of the commercial product at 0.1 V. The mass-transport overpotential, calculated per [23], is presented in Fig. 6. The 10% PAN electrospun layer produces a lower overpotential than the 12.5% PAN, whilst these both exhibit a greater mass-transport overpotential versus the commercial product. Both electrospun and commercial layers had sessile drop contact angles measured to be 140 ± 5°, see Fig. 7, suggesting similar affinity for water at layer peripheries. Based on these measurements, we suspect that similar in-situ water interactions may exist at the catalyst layer-PTL and bipolar plate-PTL interfaces, and therefore our observed differences in mass-transport overpotential might be attributable to bulk phenomena within the layers (e.g.: internal water distribution, effective diffusivities, etc.). Further diagnosis is beyond the scope of the present study; the structure–property-performance relationship remains a contemporary challenge in the PEM fuel cell community.

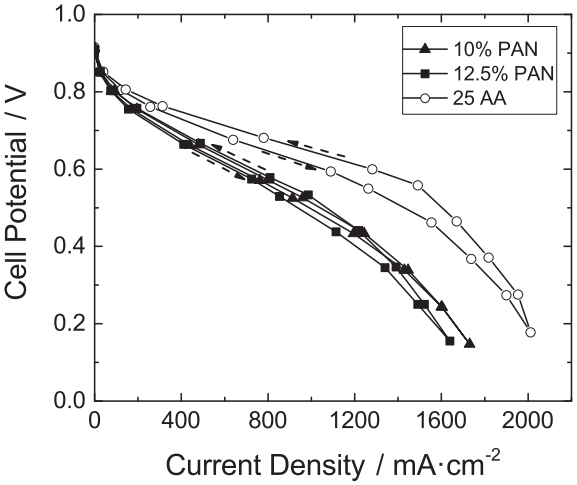

Fig. 5. Polarization curves of MEAs featuring cathode PTLs manufactured via electrospinning; also included are results of an MEA featuring a commercial cathode PTL.

Further comparing electrospun and commercial products, there is greater hysteresis in the forwards and backwards polarization curve sweeps of the commercial MEA. Progressing with a step-wise polarization curve from high-to-low average current densities requires at each new step the expulsion of excess water from the previous step(s). This excess water better hydrates the ionomer phase, producing a transient of higher performance. As the equilibration time allotted at a given step is consistent for electrospun and commercial layers; the smaller difference between forwards and reverse sweeps for the electrospun layers suggests this excess water condition is more quickly alleviated. Assuming similar water saturation at the limiting current, we posit that the commercial cathode transport layer has a higher tendency to retain water (e.g. a slower evacuation of liquid water from the MEA when approaching equilibrium at a new operating point). Depending on the application, the longer retention may or may not be a desirable behaviour, e.g. in a shutdown procedure drying of the MEA of water can be desirable to avoid ice-damage in freezing climates. Not depicted in Fig. 5, but observed during testing, was a greater propensity for cell flooding with the commercial transport layer versus the electrospun layers. Fig. 8 presents polarization curves including time-series information in quantile form. The bounds represented by the boxes and whiskers represent the 5, 25, 50, 75 and 95% quantiles of the observed current densities at a given potentiostatic set-point. Distributions of current densities are skewed toward lower current densities due to flooding events which produce transients of lower current density; as the average current density increases, so does water production, and the width of distributions increase. The electrospun PTL equipped MEA has a demonstrably narrower distribution versus the commercial product; this is reinforced in the inset of Fig. 8 which plots current density histograms and associated Weibull distributions. In real applications, the greater fuel cell operating point stability conferred by electrospun PTLs may simplify control algorithms and regulating electronics.

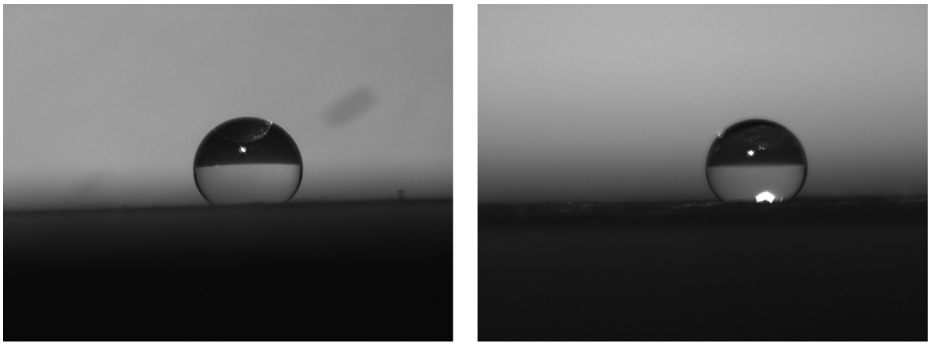

Fig. 7. Images of sessile drop contact angle measurement (a) 10% PAN electrospun and (b) commercial PTL. The observed contact angles of the electrospun (10% and 12.5% PAN) and commercial PTLs were indistinguishable at 140 ± 5°.

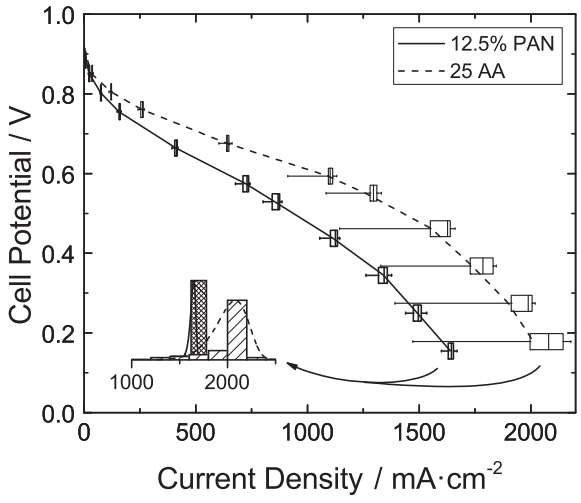

Fig. 8. Polarization data of 12.5% PAN electrospun and commercial PTLs presented as 5, 25, 50, 75 and 95% quantiles of observed current at fixed potential. The inset plot comprises histograms and Weibull distributions of the currents densities at minimum potential. 10% PAN and reverse polarization sweep data are not presented for sake of clarity.

4. Conclusion

PEMFC transport layers were produced by the novel application of electrospinning. By varying polymer concentration in the spinning dope, control over fibre diameters in the non-woven layers was demonstrated. The materials demonstrated acceptable mechanical stability for cell assembly, whilst electrical resistances were comparable to commercial material ex-situ and in-situ. Contact angle measurements suggest similar surface hydrophobicity for electrospun and commercial materials. We demonstrate promising in-situ performance from cell tests; with electrospun layers achieving approximately 85% peak currents of the commercial baseline, faster water transport, and greater output stability. We remark that this cell had been optimized for the commercial materials, design modifications may close the performance gap. With synthesis refinements, further performance can be expected over our currently non-optimized materials. The flexibility inherent in electrospinning techniques may enable deterministic links between structure, properties, and function in PTL materials.

Acknowledgements

We would like to acknowledge the financial support of the Natural Science and Engineering Research Council (NSERC) and the equipment access offered by UBC's Advanced Fibrous Materials Laboratory under Dr. Frank Ko. We would also like to acknowledge the constructive discussion with our colleague Maximilian Schwager.

References

[1] F.K. Ko, in: Y. Gogotsi (Ed.), Nanotubes and Nanofibers, CRC Press, Boca Raton, FL, 2006.
[2] A.L. Andrady, Science and Technology of Polymer Nanofibers, John Wiley & Sons, Hoboken, NJ, 2008.
[3] J.-H. Park, Y.-W. Ju, S.-H. Park, H.-R. Jung, K.-S. Yang, W.-J. Lee, J. Appl. Electrochem. 39 (2009) 1229.
[4] S.L. Singer, Low Platinum Loading Electrospun Electrodes for Proton Exchange Membrane Fuel Cells, Massachusetts Institute of Technology, 2004.
[5] J.J. Sightler, E. McPherson, W.A. Rigdon, X. Huang, ECS Trans. 50 (2013) 1445.
[6] W. Zhang, M.W. Brodt, P.N. Pintauro, ECS Trans. (2011) 891–899.
[7] J.P. Kurpiewski, Electrospun Carbon Nanofiber Electrodes Decorated with Palladium Metal Nanoparticles: Fabrication and Characterization, Massachusetts Institute of Technology, 2005.
[8] J.B. Ballengee, P.N. Pintauro, J. Electrochem. Soc. 158 (2011) B568.
[9] K.M. Lee, J. Choi, R. Wycisk, P.N. Pintauro, P. Mather, ECS Trans., ECS (2009) 1451–1458.
[10] T. Tamura, H. Kawakami, Nano Lett. 10 (2010) 1324.
[11] S. Cavaliere, S. Subianto, I. Savych, D.J. Jones, J. Rozière, Energy Environ. Sci. 4 (2011) 4761.
[12] Z. Dong, S.J. Kennedy, Y. Wu, J. Power Sources 196 (2011) 4886.
[13] J.H. Chun, K.T. Park, D.H. Jo, J.Y. Lee, S.G. Kim, S.H. Park, E.S. Lee, J.-Y. Jyoung, S.H. Kim, Int. J. Hydrogen Energy 36 (2011) 8422.
[14] H. Tang, S. Wang, M. Pan, R. Yuan, J. Power Sources 166 (2007) 41.
[15] A.M. Kannan, L. Cindrella, L. Munukutla, Electrochim. Acta 53 (2008) 2416.
[16] F.-B. Weng, C.-Y. Hsu, M.-C. Su, Int. J. Hydrogen Energy 36 (2011) 13708.
[17] D.L. Wood, R. Mukundan, R. Borup, ECS Trans., ECS (2009) 1495–1506.
[18] Q. Duan, B. Wang, J. Wang, H. Wang, Y. Lu, J. Power Sources 195 (2010) 8189.
[19] C.-J. Hung, C.-H. Liu, T.-H. Ko, W.-H. Chen, S.-H. Cheng, W.-S. Chen, A. Yu, A.M. Kannan, J. Power Sources 221 (2013) 134.
[20] M. Mathias, J. Roth, J. Fleming, W. Lehnert, in: W. Vielstich, A. Lamm, H.A. Gasteiger (Eds.), Handbook of Fuel Cells – Fundamentals, Technology, Applications, John Wiley and Sons, Chichester, England, 2003, pp. 517–537.
[21] W. Mérida, in: H. Wang, H. Li, X.-Z. Yuan (Eds.), PEM Fuel Cell Failure Mode Analysis, CRC Press, Boca Raton, FL, 2011.
[22] E.J. Ra, K.H. An, K.K. Kim, S.Y. Jeong, Y.H. Lee, Chem. Phys. Lett. 413 (2005) 188.
[23] J. Kim, S.-M. Lee, S. Srinivasan, C.E. Chamberlin, J. Electrochem. Soc. 142 (1995) 2670.